Self-driven visible-blind photodetector based on ferroelectric perovskite oxides

Jian-kun Li, Chen Ge, Kui-juan Jin, Jian-yu Du, Jing-ting Yang, Hui-bin Lu, and Guo-zhen Yang

Citation: Appl. Phys. Lett. **110**, 142901 (2017); doi: 10.1063/1.4979587
View online: http://dx.doi.org/10.1063/1.4979587
View Table of Contents: http://aip.scitation.org/toc/apl/110/14
Published by the American Institute of Physics

Self-driven visible-blind photodetector based on ferroelectric perovskite oxides

Jian-kun Li,[1,2] Chen Ge,[1,a)] Kui-juan Jin,[1,2,3,a)] Jian-yu Du,[1] Jing-ting Yang,[1] Hui-bin Lu,[1] and Guo-zhen Yang[1,2,3]
[1]*Institute of Physics, Chinese Academy of Sciences, Beijing 100190, China*
[2]*University of Chinese Academy of Sciences, Beijing 100049, China*
[3]*Collaborative Innovation Center of Quantum Matter, Beijing 100190, China*

(Received 1 December 2016; accepted 20 March 2017; published online 4 April 2017)

Ultraviolet photodetectors have attracted considerable interest for a variety of applications in health, industry, and science areas. Self-driven visible-blind photodetectors represent an appealing type of sensor, due to the reduced size and high flexibility. In this work, we employed $BaTiO_3$ (BTO) single crystals with a bandgap of 3.2 eV for the realization of a self-driven ultraviolet detector, by utilizing the ferroelectric properties of BTO. We found that the sign of the photocurrent can be reversed by flipping the ferroelectric polarization, which makes the photodetector suitable for electrical manipulation. The photoelectric performance of this photodetector was systematically investigated in terms of rectification character, stability of short-circuit photocurrent, spectral response, and transient photoelectric response. Particularly, the self-driven photodetectors based on BTO showed an ultrafast response time about 200 ps. It is expected that the present work can provide a route for the design of photodetectors based on ferroelectric oxides. *Published by AIP Publishing.*
[http://dx.doi.org/10.1063/1.4979587]

Ultraviolet (UV) photodetectors are devices that can capture UV light and convert it into electric signals. Such devices have recently attracted a great deal of attention for their broad potential applications in health, industry, and science areas, including medicine, space exploration, environmental monitoring, astronomy, and security communications.[1–3] In terms of nomenclature, detectors with a response wavelength shorter than 400 nm are called visible-blind UV photodetectors, and detectors whose response wavelength is shorter than 280 nm are called solar-blind UV photodetectors.[4,5] So far, a variety of materials have been investigated for the fabrication of these devices, such as perovskite oxides,[6,7] ZnO,[8] GaN,[9] and SiC,[10] in the form of bulk materials or thin films as well as a number of different materials in the form of quantum dots.[11,12] In a UV photodetector, the incident UV light with the photon energy higher than the bandgap of the detector material is absorbed to excite electrons from the valence band to the conduction band. Usually, in common UV photodetectors, the photogenerated electrons and holes are separated by the electric field of the supplied bias in the photoconduction mode to form photocurrent signals. This working condition, however, requires external power sources and supplies, which make the systems bulky and heavy.

Self-driven light sensors represent a type of sensor which does not require external energy inputs. These sensors can convert the incident light into electrical signals on their own, by absorbing the energy of the detected light, which allows the development of simpler equipment structures and more flexible scopes of application.[13–15] The self-driven UV detecting methods based on the electric field in the space charge region of a *p-n* junction[16,17] or the Schottky barrier[18] have been studied so far. Bie *et al.*[19] studied *p-n* junction-based self-powered visible-blind UV detectors with high sensitivity, by fabricating junctions of a single *n*-type ZnO nanowire with a *p*-type GaN film. Lu *et al.*[18] fabricated self-driven UV sensors based on a ZnO/Au Schottky junction, obtaining significant improvements in the photoresponse.

The employment of ferroelectric polarization as an electron-hole separation driving force can take advantage of the fact that the electric field originating from polarization is electrically adjustable and free from the band structure.[20–22] Ferroelectric materials are endowed with a spontaneous ferroelectric polarization that can be switched between two states by using an electric field. The photovoltaic phenomenon in $BaTiO_3$ (BTO) single crystals was first reported by Chynoweth.[23] It was demonstrated that above the Curie temperature, pyroelectric currents can be produced in BTO single crystals without the applied electric field. The polarization remaining at these temperatures is ascribed to the space-charge fields at the surface. In 1975, steady-state photocurrents proportional to the light intensity were observed in melt-grown BTO.[24] More recently, UV detectors based on ferroelectric materials have received great interest. Lai *et al.*[25] and Zomorrodian *et al.*[26] employed La-doped $Pb(Zr,Ti)O_3$ (PLZT) ferroelectric epitaxial films as self-driven UV sensors by exploiting ferroelectric polarization. In addition, since the bandgap of ferroelectric materials is generally located in the UV region, ferroelectric materials are natural candidates to perform as ideal UV photodetector materials. By employing ferroelectrics as the absorbers, photo-generated electron-hole pairs can be effectively separated by the electric field induced by spontaneous polarization. Therefore, stable photocurrents are present even in the absence of external electric fields.[27] The photocurrents increase with the intensity of the incident light, which can allow achieving the purpose of UV detection.

[a)]Authors to whom correspondence should be addressed. Electronic addresses: gechen@iphy.ac.cn and kjjin@iphy.ac.cn

As a result, ferroelectrics-based UV detectors provide great potential in device design and preparation and show more prominent advantages in conditions of limited available power such as space or underwater environment.

In the present work, we demonstrate the realization of a self-driven visible-blind UV photodetector based on a ferroelectric BTO single crystal. The cutoff wavelength of BTO single crystals in our experiment is approximately 392 nm, corresponding to a bandgap of about 3.2 eV. Therefore, BTO can work in the absence of filters to block visible light. Moreover, BTO is an ideal photovoltaic material with a high Curie temperature, excellent chemical stability, and thermal stability. In our experiments, a sandwich-type metal/BTO/metal structure is fabricated for photoelectric measurements. The open-circuit voltages, short-circuit currents, ultrafast responses of unpolarized BTO, negative polarized BTO, and positive polarized BTO were measured in our experiments, finding stable open-circuit voltages, short-circuit currents, ultrafast zero-bias responses, and recovery times. Our experiment results indicate that ferroelectric BTO is suitable for the preparation of self-driven visible-blind UV detectors.

As shown in Fig. 1(a), commercial unpolarized BTO single crystals (MTI Corporation) with a size of $5 \times 5 \times 0.5\,\text{mm}^3$ were prepared for photoelectric measurements. Au top electrodes with a diameter of 420 μm and a thickness of 100 nm were deposited on the BTO wafers by thermal evaporation. Silver paint electrodes were applied to the bottom of the wafers to perform the measurements. Since the photo-ferroelectric effect is proportional to polarization for ferroelectric materials, a large external electric field of ± 42 kV/cm was applied for 500 s to flip the electric polarization. For convenience, the unpolarized BTO sample is labeled as *UN-BTO*, the downward polarized BTO sample is labeled as *DOWN-BTO*, and the upward polarized BTO sample is labeled as *UP-BTO*.

Figure 1(b) displays the parallel view of two atomic structure schematic diagrams of *DOWN-BTO* (left) and *UP-BTO* (right) in the tetragonal phase at room temperature, in which the displacement of the titanium atom is exaggerated. The hybridization between the Ti 3 d states and the O 2 p states leads to the displacement of Ti atoms, which makes the BTO crystals ferroelectric.[28]

Figure 1(c) shows a typical polarization-electric field (P-E) hysteresis loop for the BTO single crystal at 2 Hz with a field amplitude value of 44 kV/cm measured by a piezoelectric test system (Radiant RT6000HVS), which confirms the good ferroelectric properties of the BTO samples. A remnant polarization of 23 μC/cm^2 and coercive field amplitudes of -28.4 kV/cm and $+21.8$ kV/cm were observed at room temperature. In order to determine the bandgap of BTO, the absorption and transmission spectra of *UN-BTO* were measured, as shown in Fig. 1(d). The transmission edge is located at about 392 nm, which is a little smaller than the edge of the visible light wavelength range (400 nm), indicating the effective coverage of UV light and shielding of visible light. The bandgap obtained from the transmission spectrum is about 3.2 eV. In order to identify the polarized domains of BTO samples, we achieved polarization patterns of *UN-BTO* and *DOWN-BTO* by the piezoreponse force microscopy (PFM) technique (Asylum Research MFP-3D) as displayed in Figs. 1(e) and 1(f). The PFM images were collected along the out-of-plane direction over $10 \times 10\,\mu\text{m}^2$ areas. In *UN-BTO*, irregular ferroelectric domains with different polarization directions can be clearly observed as shown in Fig. 1(e). However, as can be seen from Fig. 1(f),

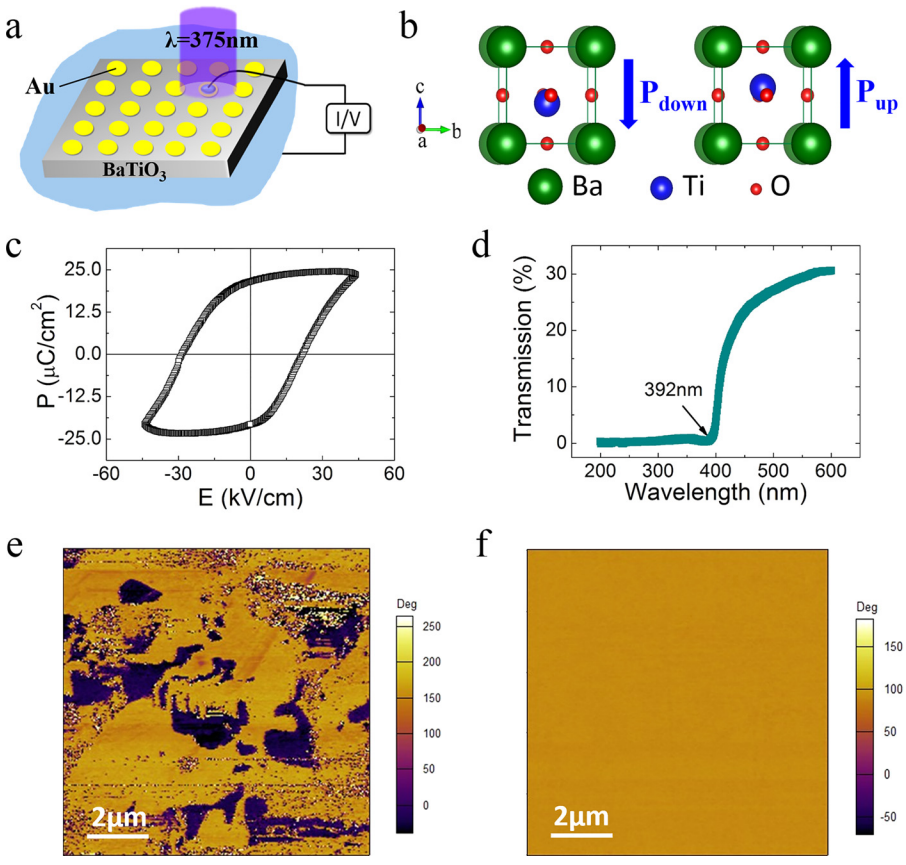

FIG. 1. (a) Sketch of the setup for electrode covered BTO single crystal, incident UV laser, and measuring circuit. (b) Parallel view of the atomic structure schematic diagrams for *DOWN-BTO* (left) and *UP-BTO* (right). The blue arrows represent the direction of polarizations. The Ba, Ti, and O sites are displayed by green, blue, and right circles, respectively. (c) Typical polarization-electric field loops of BTO with 2 Hz frequency, indicating a remnant polarization of 23 μC/cm and coercive fields of -28.4 kV/cm and $+21.8$ kV/cm. The value of the field amplitude is 44 kV/cm. (d) Transmission spectra of *UN-BTO*. (e) and (f) Images of out-of-plane PFM for *UN-BTO* before (e) and after (f) $+42$ kV/cm polarization process over $10 \times 10\,\mu\text{m}^2$ areas. The images show that $+42$ kV/cm electric field induces a homogeneous state with downward polarization.

only one polarization direction is present in *DOWN-BTO* after the application of the external electric field. The comparison between the two PFM panels indicates that our polarization method can effectively change the polarization direction of BTO.

The photovoltaic characteristics of *UN-BTO*, *DOWN-BTO*, and *UP-BTO* were studied in a sandwich electrode configuration under continuous UV laser illumination with a wavelength of 375 nm, and the results are respectively shown in Figs. 2(a)–2(c). The experimental data were collected by a Keithley 4200 A-SCS. The corresponding open-circuit voltage and short-circuit current density of the three samples illuminated with different light intensities are shown in Figs. 2(d)–2(f), respectively. Current density-voltage (J-V) curves of *UN-BTO* displayed rectification characteristics as shown in Fig. 2(a). The maximum applied bias is 1 V (20 V/cm) for the three samples, which is far below the coercive field for polarization switching. Open-circuit voltage and short-circuit current are almost unaffected by variations of the light intensity (Fig. 2(d)). Figures 2(b) and 2(c) show the rectifying curves of *DOWN-BTO* and *UP-BTO* in the dark environment and under laser illumination, respectively. From the measurements, we obtained an open-circuit voltage of $V_{oc} \approx 0.7$ V and $V_{oc} \approx -0.6$ V for *DOWN-BTO* and *UP-BTO*, respectively. These open-circuit voltages are almost independent of light intensity. The corresponding photo-induced open-circuit electric field is about 14 (−12) V/cm for *DOWN-BTO* (*UP-BTO*). In the light intensity range of 0–8.05 mW/mm^2, the values of the short-circuit current density (J_{sc}) of *DOWN-BTO* and *UP-BTO* increase monotonically with increasing laser intensity (see Fig. 2(e)–2(f)). J_{sc} values for the two samples are up to −111 nA/cm^2 and 136 nA/cm^2, respectively, at an incident laser power density of 8.05 mW/mm^2.

The photoelectric behaviors of the *UN-BTO*, *DOWN-BTO*, and *UP-BTO* are closely related to the polarization direction.[29] In *UN-BTO*, since the micron-scale ferroelectric domains are randomly distributed, almost no ferroelectricity is observed at a macroscopic level. Therefore, no open-circuit voltage and short-circuit current were detected in *UN-BTO* (Fig. 3(a)). After a +42 kV/cm electric field applied to the top electrode of *DOWN-BTO* for 500 s, a ferroelectric polarization is formed in the downward direction and caused the existence of the additional dipole layer close to the electrodes. In other words, as depicted in Fig. 3(b), the comprehensive effect of depolarized electric field E_{de} (purple arrow) and dipole layers close to the electrodes (represented by the plus sign and minus sign in Fig. 3(b)) resulted in a measurable open-circuit electric field of 14 V/cm. The photo-generated holes (white circles with a plus sign in Fig. 3(b)) and electrons (black circles with a minus sign in Fig. 3(b)) are separated by E_{de}, and a short-circuit current density of −111 nA/cm^2 is measured under the 375 nm UV laser illumination with a light intensity of 8.05 mW/mm^2. If a −42 kV/cm electric field is applied to *UP-BTO*, ferroelectric polarization points to the upward direction, and the polarity of the charge layer is reversed. Under the action of E_{de} and dipole layers, an open-circuit electric field of −12 V/cm and a short-circuit current density of 136 nA/cm^2 are measured in *UP-BTO*.

In order to assess the photoelectric performance of our photodetectors, we also investigate important parameters such as the external quantum efficiency (EQE) and the detectivity D*. The EQE η_{eqe} under short-circuit conditions was calculated for *DOWN-BTO* and *UP-BTO*. This quantity is defined as the number of carriers generated per incoming photon

$$\eta_{\mathrm{eqe}} = \mathrm{R}_i h\omega/e, \tag{1}$$

where R_i is the spectral current responsivity at the selected wavelength, h is Planck's constant, and ω is the frequency of the incident light. Accordingly, at an incident photon wavelength $\lambda = 375$ nm, the η_{eqe} of *DOWN-BTO* and *UP-BTO* is, respectively, $4.56 \times 10^{-5}\%$ and $4.41 \times 10^{-5}\%$ if surface reflection is not taken into account. The quantum efficiencies of ferroelectric visible-blind detectors working at zero bias are $\eta \sim 3.51 \times 10^{-5}\%$ for $PbTiO_3$ and $\eta \sim 4.42 \times 10^{-6}\%$ for La-doped Pb(Zr,Ti)O_3.[26,30] For non-ferroelectric visible-blind detectors, the quantum efficiencies are $\eta \sim 5.4\%$ for ZnO and $\eta \sim 14.7\%$ for the TiO_2/SnO_2 branched heterojunction nanostructure.[31,32] The quantum efficiency of our device is higher than those of other ferroelectric oxides, but lower than those of conventional semiconductors, possibly due to the relatively poor crystal quality.

The detectivity D* is also a widely used parameter characterizing the normalized signal-to-noise performance of detectors, and it can be defined as follows:

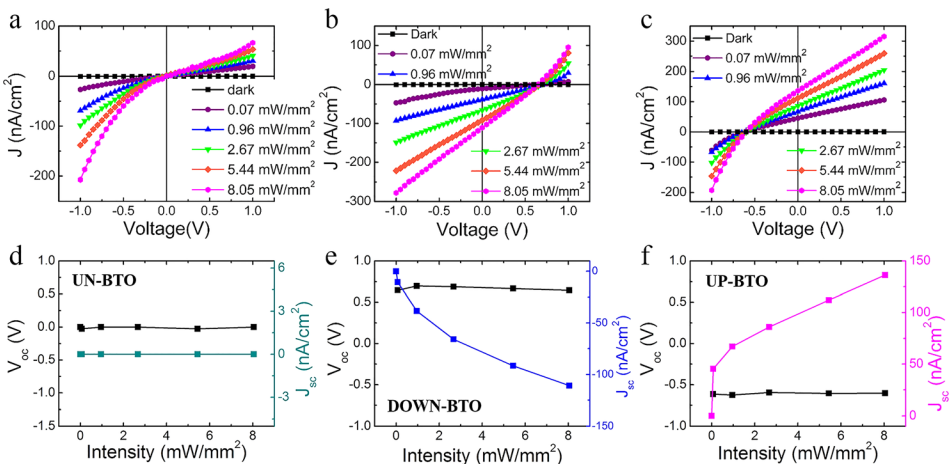

FIG. 2. The photocurrent density dependence of voltage bias for *UN-BTO* (a), *DOWN-BTO* (b), and *UP-BTO* (c) using different light intensities. The open-circuit voltages and short-circuit currents density with different light intensities of *UN-BTO*, *DOWN-BTO*, and *UP-BTO* are shown in (d), (e), and (f), respectively.

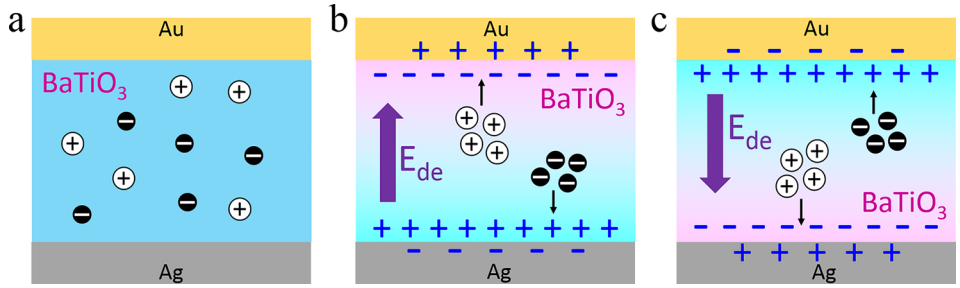

FIG. 3. (a) Schematic diagram of distribution of photo-generated charge in *UN-BTO*. The photo-generated holes (white circles with plus sign in center) and electrons (black circles with minus sign in center) are randomly distributed without external bias. (b) and (c) Causes of open-circuit voltage and short-circuit current in *DOWN-BTO* (b) and *UP-BTO* (c). With the comprehensive effect of depolarized electric field (purple arrow) and dipole layers close to the electrodes (represented by the plus sign and minus sign in (b) and (c)), open-circuit voltages are detected and photo-generated carriers are oriented to form short-circuit currents.

$$D^* = (A\Delta f)^{1/2} R_i / I_n, \tag{2}$$

where A is the effective area of the device, Δf is the frequency band, and I_n is the noise current source.

There are three sources of noises that contribute to lowering D^*: shot noise from dark current, Johnson noise, and thermal fluctuation "flicker" noise. As the thermally limited mode is not applied,[33] shot noise is the main source of noise in our experiment.

I_n is given by the following relation:

$$I_n = \left(\frac{4k_B T}{R_{dark}} + 2qI_{dark}\right)^{1/2} \Delta f^{1/2}, \tag{3}$$

where T is the temperature, R_{dark} is the differential resistance at the bias point, I_{dark} is the zero-bias dark current, k_B is Boltzmann's constant, and q is the electron charge. Non-zero short-circuit currents are presented in the dark. The low dark data at zero-bias may be caused by instrument noise. Therefore, the detectivity is meaningless at zero bias. In order to test the detector performance of our samples, we calculated the detectivities at 1 V bias. According to Equations (2) and (3), the D^* of *DOWN-BTO* and *UP-BTO* under light illumination with a wavelength of 375 nm was found to be 1.56×10^8 cm · Hz$^{0.5}$/W and 1.05×10^8 cm · Hz$^{0.5}$/W, respectively.

Figure 4(a) shows time-resolved measurements of the short-circuit photocurrent density as the light is switched on and off for our *UN-BTO*, *DOWN-BTO*, and *UP-BTO* samples. The current strongly depends on the ON/OFF switching of the 375 nm UV laser, and its value becomes larger with the increase in the incident light intensity. In order to investigate the stability of *DOWN-BTO* and *UP-BTO*, the steady state short-circuit photocurrent density responses of *DOWN-BTO* and *UP-BTO* were measured for over 10^4 s as shown in Fig. 4(b), indicating good stability over time.

As shown in Fig. 4(c), the transient photoelectric response behaviors of *UN-BTO*, *DOWN-BTO*, and *UP-BTO* were acquired at zero bias by a 2.5 GHz bandwidth oscilloscope and a 355 nm UV laser with a pulse duration of 18 ps. A 0.5 Ω resistance was connected in parallel with the samples. Almost no photovoltaic signal was detected for *UN-BTO*. However, for *DOWN-BTO* and *UP-BTO*, the measured photovoltages were −33.6 mV and 37.8 mV, respectively. The rise time and full width at half maximum (FWHM) were 270 ps and 310 ps for *DOWN-BTO* and 220 ps and 230 ps for *UP-BTO*, respectively. The faster response and recovery times confirmed the low carrier transit time and the rapid electron-hole pair recombination process in BTO crystals. Compared with other oxide materials such as ZnO,[19] $LiNbO_3$,[34] and $KTaO_3$,[35] polarized BTO crystals displayed

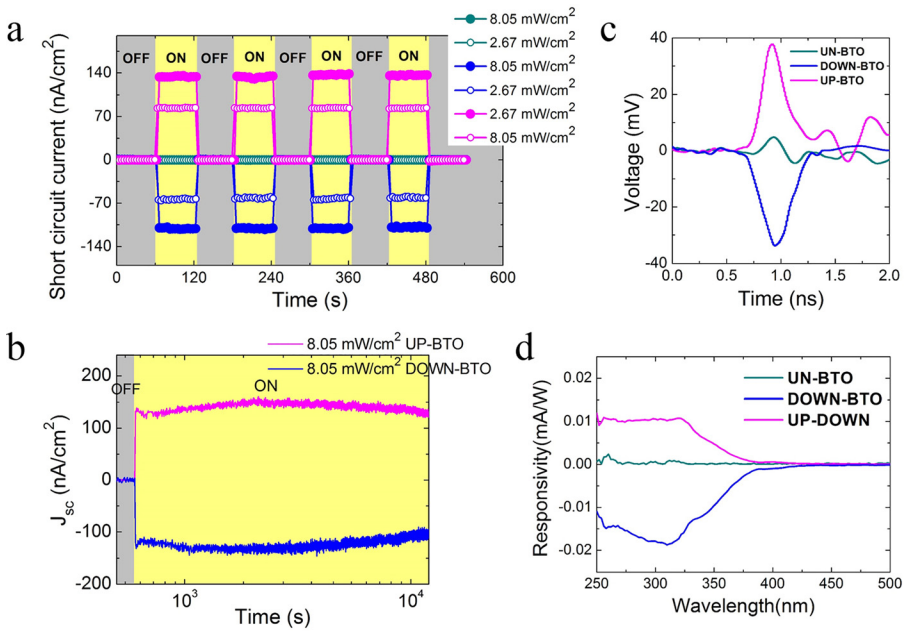

FIG. 4. (a) J_{sc} of *UN-BTO* (green), *DOWN-BTO* (blue), and *UP-BTO* (magenta) crystal under a continuous 375 nm UV laser, with periodic on/off states. (b) Steady-state J_{sc} responses of *DOWN-BTO* and *UP-BTO*. (c) Transient photoelectric responses of *UN-BTO*, *DOWN-BTO*, and positive *UP-BTO* without voltage bias. The experiment results were measured by a 2.5 GHz bandwidth oscilloscope and a 355 nm laser with the pulse width of 18 ps. (d) Spectral responses of the *UN-BTO*, *DOWN-BTO*, and *UP-BTO* at 0 V bias.

ultrafast response. As a key factor for detection performance, the ultrafast response time can naturally expand the application possibilities of BTO.

Figure 4(d) represents the spectral responses of *UN-BTO* (green), *DOWN-BTO* (blue), and *UP-BTO* (magenta) at zero bias. There is almost no short-circuit current in *UN-BTO*, regardless of the wavelength. Conversely, *DOWN-BTO* and *UP-BTO* exhibit a cutoff wavelength of 388 nm, consistently with the ~3.2 eV bandgap of BTO. When the wavelength is lower than the cutoff wavelength, the responsivity increases with decreasing wavelength, until saturation at 320 nm with a photocurrent responsivity of 0.01 mA/W. We define the UV-to-visible contrast ratio as the ratio of the responsivity measured at 320 nm to the responsivity measured at 400 nm. The UV-to-visible contrast ratio, which indicates the signal-to-noise ratio, is about 15 for *DOWN-BTO* and 20 for *UP-BTO*.

In summary, we employed BTO as a promising ferroelectric material for self-driven visible-blind UV detecting. The absorption edge and transmission edge are at about 390 nm, indicating activities in the UV range. With the modulation of polarization direction, stable photocurrents in different directions are found in the absence of external electric fields due to the ferroelectric polarization in BTO and become larger as the intensity of the incident light increases. An ultrafast response time and a FWHM of ~200 ps were observed in our samples, indicating the feasibility and the unique potential of BTO for UV detection applications. These results indicate that BTO crystals are promising self-driven UV detecting candidates for future applications.

This work was supported by the National Basic Research Program of China (No. 2014CB921001), the National Hi-tech (R&D) project of China (No. 2014AA032607), the National Natural Science Foundation of China (Nos. 11674385 and 11404380), the Key Research Program of Frontier Sciences, CAS (No. QYZDJ-SSW-SLH020), and the Strategic Priority Research Program (B) of the Chinese Academy of Sciences (No. XDB07030200).

[1]M. Razeghi and A. Rogalski, J. Appl. Phys. **79**(10), 7433 (1996).
[2]Z. L. Wang, Adv. Mater. **24**(2), 280–285 (2012).
[3]Z. Lou, L. D. Li, and G. Z. Shen, Nano Res. **8**(7), 2162–2169 (2015).
[4]X. L. Zhao, Z. P. Wu, D. Y. Guo, W. Cui, P. G. Li, Y. H. An, L. H. Li, and W. H. Tang, Semicond. Sci. Technol. **31**(6), 065010 (2016).
[5]M. L. Ai, D. Y. Guo, Y. Y. Qu, W. Cui, Z. P. Wu, P. G. Li, L. H. Li, and W. H. Tang, J. Alloys compd. **692**, 634–638 (2016).
[6]H. W. Chen, N. Sakai, A. K. Jena, Y. Sanehira, M. Ikegami, K. C. Ho, and T. Miyasaka, J. Phys. Chem. Lett. **6**(9), 1773–1779 (2015).
[7]G. Maculan, A. D. Sheikh, A. L. Abdelhady, M. I. Saidaminov, M. A. Haque, B. Murali, E. Alarousu, O. F. Mohammed, T. Wu, and O. M. Bakr, J. Phys. Chem. Lett. **6**(19), 3781–3786 (2015).
[8]M. Laurenti, G. Canavese, A. Sacco, M. Fontana, K. Bejtka, M. Castellino, C. F. Pirri, and V. Cauda, Adv. Mater. **27**(28), 4218–4223 (2015).
[9]D. B. Li, X. J. Sun, H. Song, Z. M. Li, H. Jiang, Y. R. Chen, G. Q. Miao, and B. Shen, Appl. Phys. Lett. **99**(26), 261102 (2011).
[10]A. Sciuto, F. Roccaforte, S. D. Franco, V. Raineri, and G. Bonanno, Appl. Phys. Lett. **89**(8), 081111 (2006).
[11]Y. Z. Jin, J. P. Wang, B. Q. Sun, J. C. Blakesley, and N. C. Greenham, Nano Lett. **8**(6), 1649–1653 (2008).
[12]F. W. Guo, B. Yang, Y. B. Yuan, Z. G. Xiao, Q. F. Dong, Y. Bi, and J. S. Huang, Nat. Nanotechnol. **7**(12), 798–802 (2012).
[13]X. J. Hou, B. Liu, X. F. Wang, Z. R. Wang, Q. F. Wang, D. Chen, and G. Z. Shen, Nanoscale **5**(17), 7831–7837 (2013).
[14]J. Ding, H. J. Fang, Z. P. Lian, J. W. Li, Q. R. Lv, L. D. Wang, J. L. Sun, and Q. F. Yan, Cryst. Eng. Commun. **18**(23), 4405–4411 (2016).
[15]B. K. Gan, K. Yao, S. C. Lai, P. C. Goh, and Y. F. Chen, IEEE Electron Device Lett. **32**(5), 665–667 (2011).
[16]T. Palacios, E. Monroy, F. Calle, and F. Omnès, Appl. Phys. Lett. **81**(10), 1902 (2002).
[17]Q. Chen, M. A. Khan, and J. W. Yang, Electron. Lett. **31**(20), 1781–1782 (1995).
[18]S. N. Lu, J. J. Qi, S. Liu, Z. Zhang, Z. Z. Wang, P. Lin, Q. L. Liao, Q. j. Liang, and Y. Zhang, ACS Appl. Mater. Interfeces **6**(16), 14116–14122 (2014).
[19]Y. Q. Bie, Z. M. Liao, H. Z. Zhang, G. R. Li, Y. Ye, Y. B. Zhou, J. Xu, Z. X. Qin, L. Dai, and D. P. Yu, Adv. Mater. **23**(5), 649–653 (2011).
[20]L. Z. Tan, F. Zheng, S. M. Young, F. Wang, S. Liu, and A. M. Rappe, NPJ Comput. Mater. **2**, 16026 (2016).
[21]M. R. Morris, S. R. Pendlebury, J. Hong, S. Dunn, and J. R. Durrant, Adv. Mater. **28**(33), 7123–7128 (2016).
[22]B. K. Gan, K. Yao, S. C. Lai, Y. F. Chen, and P. C. Goh, IEEE Electron Device Lett. **29**(11), 1215–1217 (2008).
[23]A. G. Chynoweth, Phys. Rev. **102**, 705 (1956).
[24]W. T. H. Koch, R. Munser, W. Ruppel, and P. Würfel, Solid State Commun. **17**, 847 (1975).
[25]S. C. Lai, K. Yao, Y. F. Chen, L. Zhang, and Y. F. Lim, IEEE Electron Device Lett. **34**(11), 1427–1429 (2013).
[26]A. Zomorrodian, N. J. Wu, Y. Song, S. Stahl, A. Ignatiev, E. B. Trexler, and C. A. Garcia, Jpn. J. Appl. Phys., Part 2 **44**, 6105–6108 (2005).
[27]C. J. Won, Y. A. Park, K. D. Lee, H. Y. Ryu, and N. Hur, J. Appl. Phys. **109**(8), 084108 (2011).
[28]R. E. Cohen, Nature **358**(9), 136–138 (1992).
[29]C. Ge, K. J. Jin, C. Wang, H. B. Lu, C. Wang, and G. Z. Yang, Appl. Phys. Lett. **99**, 063509 (2011).
[30]K. Uchino, Y. Miyazawa, and S. Nomura, Jpn. J. Appl. Phys., Part 2 **21**, 1671–1674 (1982).
[31]O. Game, U. Singh, T. Kumari, A. Banpurkar, and S. Ogale, Nanoscale **6**, 503–513 (2014).
[32]X. Li, C. Gao, H. Duan, B. Lu, Y. Wang, L. Chen, Z. Zhang, X. Pan, and E. Xie, Small **9**(11), 2005–2011 (2013).
[33]T. Choi, S. Lee, Y. J. Choi, V. Kiryukhin, and S. W. Cheong, Science **324**(3), 63–67 (2009).
[34]E. J. Guo, J. Xing, K. J. Jin, H. B. Lu, J. Wen, and G. Z. Yang, J. Appl. Phys. **106**(2), 023114 (2009).
[35]J. T. Yang, C. Ge, K. J. Jin, H. B. Lu, and G. Z. Yang, Appl. Opt. **55**(9), 2259–2262 (2016).